Environmental Fluid Mechanics **1:** 311–332, 2001.

A Numerical Study of the Dynamics of the Riverine Thermal Bar in a Deep Lake

PAUL R. HOLLAND, ANTHONY KAY* and VINCENZO BOTTE
Department of Mathematical Sciences, Loughborough University, Loughborough, Leicestershire, LE11 3TU, U.K.

Received 21 March 2001; accepted in revised form 6 August 2001

Abstract. A numerical model based on a Finite Volume formulation of the Navier–Stokes equations is used to simulate a range of scenarios leading to a thermal bar formed by a river inflow to an idealised deep lake. The results presented here show that small riverine salinity increases have a profound effect on the dynamics of the thermal bar, suppressing horizontal propagation of the plume and raising the possibility of a thermal bar which is capable of sinking to great depths. This finding is particularly relevant to Lake Baikal in Siberia, where the vigorous deep-water renewal is still not fully understood. An analysis of the buoyancy forces governing the depth of penetration of the thermal bar plume shows that realistic salinity gradients are an important factor in determining the circulation of Baikal waters. Observations of the saline curtailment of the thermal bar's horizontal propagation also reveal a potential for reduced productivity in the ecosystem of any temperate river delta during the Spring renewal period.

Key words: buoyancy, cabbeling, deep convection, Lake Baikal, numerical modelling, river, salinity, thermal bar

1. Introduction

An important feature of the circulation of many lakes in temperate regions is the thermal bar, a downwelling plume of water which arises from the existence of a temperature of maximum density (T_{md}) in fresh water. If two bodies of fresh water on either side of the T_{md} are allowed to mix then cabbeling takes place, whereby the mixed water will be denser than both components and therefore sinks until it encounters denser water.

The classical thermal bar appears in lakes in Spring and Autumn when the surface temperature passes through the T_{md} due to radiative effects; near-shore shallow regions are affected first (since heating and cooling are fastest there) and a sinking plume of maximally dense water appears at the lake shore and migrates toward the deeper regions as the surface heat flux continues [1–3].

In contrast to this, the riverine thermal bar is generated at a river inflow where lake and river temperatures are on opposite sides of the T_{md}. In Spring, a surface heat flux will warm a relatively shallow and rapidly-mixed river through the T_{md}

*Correspondence author, E-mail: A.Kay@lboro.ac.uk

more rapidly than a deep lake, and conditions are then favourable for the formation of a thermal bar.

Lake Baikal in Eastern Siberia is the deepest (maximum depth 1632 m [4]) and oldest freshwater lake in the world, and is of global importance due to its unique ecosystem and the paleoclimatic record in its sediments, which date back some 30 million years [5]. The process of deep-water renewal, by which oxygenated water descends to the bed and nutrient-rich waters return to the surface, is crucial to both the maintenance of the ecosystem and the formation of the sediments [6].

There is plenty of evidence of large-scale vertical convective processes operating in Lake Baikal, which ensure that the entire water column exceeds 80% of relative saturation for dissolved Oxygen [7, 8]. International scientific interest is concentrated on the issue of deep-water ventilation and several possible mechanisms have been proposed, but with no consensus as yet. However, Carmack and Weiss [9] have shown that, due to the decrease of the T_{md} with increasing pressure (by about 1 °C per 500 m depth), it is not possible for the classical thermal bar plume to reach the bed of a great lake such as Baikal.

Hohmann *et al.* [10] identified the Selenga River, Baikal's largest tributary, as a major source of deep-water ventilation as a result of the saline plume it creates in early Spring prior to the onset of stable stratification. It seems reasonable therefore that as the Selenga warms through the T_{md}, the thermal bar which is generated has a chance of renewing the deeper Baikal waters due to its riverine salinity content.

In addition to promoting vertical mixing, the thermal bar is known to impede horizontal transport across its converging surface flows [11]. In the riverine case this has particularly important consequences for the transfer of enhanced riverine nutrient levels, resulting in favourable conditions for the growth of phytoplankton inshore of the thermal bar [12]. Botte and Kay [13] found that the stratification of a Baikal water column also had a marked effect on plankton concentrations. This suggests that the nutrient-rich, stable regions inshore of a riverine thermal bar could initiate the Spring phytoplankton bloom while waters offshore of the density maximum are still relatively unproductive. Therefore horizontal propagation of the riverine thermal bar could be crucial in governing the quantity and distribution of plankton in a temperate lake such as Baikal. Studies of the effect of the dynamics presented in this paper on a coupled plankton model are currently in progress.

The thermal bar driven by a surface heat flux is a relatively well-modelled phenomenon, particularly in Lake Baikal. Malm [1] carried out a full numerical study of thermal bars under a range of wind and bathymetric conditions but neglected thermobaric effects, adopting a uniform T_{md} with depth. Tsvetova [14, 15] made significant advances with a compressible model of Baikal's thermal bar but unfortunately failed to fully explore the details of thermobaric control of the sinking plume. More recently, Botte and Kay [13] briefly studied thermobaricity as part of their plankton population study in the vicinity of a Spring thermal bar in Lake Baikal.

The fundamental difference between the riverine thermal bar and its classical counterpart is the effect of riverine salinity on the density distributions which drive this phenomenon. Observations of the riverine thermal bar are available for a few Canadian lakes [16, 17], and Killworth and Carmack [18] constructed a one-dimensional 'filling-box' model of a lake with a river inflow at a seasonally varying temperature. However, to the knowledge of the authors there have been no previous attempts at modelling the effects of a range of riverine salinity and temperature distributions on the thermal bar phenomenon or the resulting circulation.

The primary intention of this study is therefore to examine the characteristics of a riverine thermal bar with and without a salinity influx from the river. In particular, we seek to determine the conditions under which the river inflow can be an agent of deep-water renewal in the lake. Purely thermal forcing is considered first, with three different temperature regimes for the river and lake representing different stages in the Spring warming. The sensitivity of the thermal bar to saline forcing is then examined by adding four different salinity excesses to the river inflow.

Since our objective is to gain a first insight into the effects of buoyancy forcings without obscuring them with site-specific boundary effects, we follow the work of several other authors [1, 19] in adopting a simplified deep-lake geometry. We also neglect Coriolis forces, again to avoid obscuring the buoyancy-driven dynamics, even though the time-scale of our model runs is several days. Studies with a longer, shallower lake model which permits simulations over longer time-scales have shown that there is a spin-up period of a few days, so it would in any case not be possible to represent Coriolis effects in a physically realistic manner in the present study.

The consequences of Spring warming in the Selenga delta are studied using a two-dimensional lake model with a throughflowing river. While the ideal model would involve a coupled river and lake which are initially cooler than the T_{md} and then subjected to a surface heat flux, the computationally intensive nature of the long runs required by this approach makes it unfeasible for the purposes of the present study. Warming of the river and lake is therefore simulated by two separate one-dimensional models under a surface heat flux. The results of these models are then used after various simulation times to provide boundary and initial conditions for the main two-dimensional mixing studies. Increasing the river salinity in certain scenarios then completes a dynamical study of a range of conditions present during the generation of a riverine thermal bar in a deep lake.

2. Governing Equations

In order to obtain the relatively fine spatial resolution required to represent the temperature gradients responsible for the thermal bar, a two-dimensional section is adopted with the justification that gradients normal to the shore are much larger than those parallel to it, which are neglected accordingly.

Cartesian coordinates x and z are defined in the plane of a rectangular section such that z represents the vertical direction, taken as positive upwards, and x increases away from the river inflow, as shown in Figures 1a and 1b. As mentioned previously, the section is chosen to be rectangular so that the predicted dynamics are independent of specific bathymetry and may be regarded as generally applicable.

This study employs a quasi-incompressible formulation of the Reynolds-averaged Navier–Stokes equations under the Boussinesq approximation [20]. The density is therefore supposed to equal the maximum density of pure water at $p = 0$, $\rho_c = 999.975$ kg m^{-3}, everywhere except in the buoyancy term. Under these assumptions the continuity equation becomes

$$\frac{\partial u}{\partial x} + \frac{\partial w}{\partial z} = 0 \tag{1}$$

and the components of the momentum equation are

$$\frac{\partial u}{\partial t} + u\frac{\partial u}{\partial x} + w\frac{\partial u}{\partial z} = \frac{\partial}{\partial x}\left(A_h \frac{\partial u}{\partial x}\right) + \frac{\partial}{\partial z}\left(A_v \frac{\partial u}{\partial z}\right) - \frac{1}{\rho_c}\frac{\partial p}{\partial x}, \tag{2}$$

$$\frac{\partial w}{\partial t} + u\frac{\partial w}{\partial x} + w\frac{\partial w}{\partial z} = \frac{\partial}{\partial x}\left(A_h \frac{\partial w}{\partial x}\right) + \frac{\partial}{\partial z}\left(A_v \frac{\partial w}{\partial z}\right) - \frac{1}{\rho_c}\frac{\partial p}{\partial z} - \frac{\rho}{\rho_c}g, \tag{3}$$

where A_h and A_v are eddy-viscosity coefficients in the horizontal and vertical directions respectively and g is the acceleration due to gravity. Density is calculated from the accurate equation of state of Chen and Millero [21], which is valid over the full ranges of p, S, and T encountered in this study.

The transport equation for a generic scalar variable Φ is simply obtained by considering a balance between convection and diffusion:

$$\frac{\partial \Phi}{\partial t} + u\frac{\partial \Phi}{\partial x} + w\frac{\partial \Phi}{\partial z} = \frac{\partial}{\partial x}\left(K_h \frac{\partial \Phi}{\partial x}\right) + \frac{\partial}{\partial z}\left(K_v \frac{\partial \Phi}{\partial z}\right), \tag{4}$$

where K_h and K_v are diffusivity coefficients for the transported quantity in each coordinate direction. In this work the scalar variables consist of temperature T, salinity S, and a tracer variable φ, which is introduced in order to quantify the transport of riverine substances by the predicted motions.

In oceanography and limnology, eddy viscosities are often crudely assumed to be constant or very simplified functions of the temperature or density fields. The chosen parameterisation is based on the formulation of Botte and Kay [13], which has been modified in this work to include the effects of salinity variation. A full justification of this model may be found in the original paper.

Static stability limits small-scale vertical motion, so vertical eddy viscosities are expressed as a function of the square of the Brunt–Väisälä frequency,

$$N^2 = g\left[\alpha\left(\frac{\partial T}{\partial z} - \Gamma\right) - \beta\frac{\partial S}{\partial z}\right], \tag{5}$$

which quantifies the strength of stratification such that $N^2 > 0$ for stable conditions [22]. Here α is the coefficient of thermal expansion, β is the coefficient of haline contraction, and Γ is the adiabatic temperature gradient.

For stable situations, Welander [23] has proposed a relation of the form:

$$A_v = a(N^2)^b \tag{6}$$

where a and b are constants. The adopted model is based upon this formulation and is completed by assigning constant values to A_v for unstable and very stable situations:

$$A_v = \begin{cases} 0.0004 + 6 \times 10^{-7}(N^2)^{-0.5} \text{ m}^2 \text{ s}^{-1} & N^2 > N^2_{\text{min}}, \\ 0.02 \text{ m}^2 \text{ s}^{-1} & N^2 \leq N^2_{\text{min}}, \end{cases} \tag{7}$$

where a cut-off value for stable conditions, $N^2_{\text{min}} = 9.371 \times 10^{-10} \text{ s}^{-2}$, has been introduced in order to avoid large values of A_v as $N^2 \to 0$. All parameter values in this expression are chosen by fitting model results to vertical temperature profiles from Lake Baikal during the Spring warming period, as described by Botte and Kay [13].

Horizontal eddy-viscosities are usually simply assigned a constant value, and a wide range of values is present in the literature. In reality the horizontal eddy-viscosity plays an important role in suppressing the spurious motions which arise from aliasing problems due to the coarseness of the chosen grid [24], and therefore the exact value of A_h is chosen more for this purpose rather than from consideration of physical processes. In this work a value of $A_h = 5 \text{ m}^2 \text{ s}^{-1}$ has been adopted on the sole basis that it seems to suppress most of the spurious motions while providing a reasonable horizontal mixing, without excessive damping of the flow-field. Values of both A_h and A_v were chosen following a sensitivity analysis, details of which are given by Holland [25].

Eddy diffusivities K_h and K_v are chosen to be the same as A_h and A_v because this is the most reasonable assumption in the absence of any other information.

Equations (1)–(4) are solved numerically on a staggered grid using a non-hydrostatic Finite Volume formulation which employs a pressure correction procedure similar to the SIMPLE scheme of Patankar [26]. The reader is again referred to the work of Botte and Kay [13] for a full description of the solution process.

The computational domain is taken to be a rectangle of length $L = 6$ km and depth $D = 1000$ m, discretised using a uniform mesh which has cell dimensions of $h_x = 20$ m by $h_z = 5$ m. This gives a total number of cells of 300×200, which corresponds to the maximum number of grid points that can be used with the computational resources available to this study. River inflow and outflow regions are taken to be 50 m-deep open sections at the top of the side boundaries; the inflow and outflow depths are kept equal to prevent the generation of spurious vertical velocities by the boundary conditions.

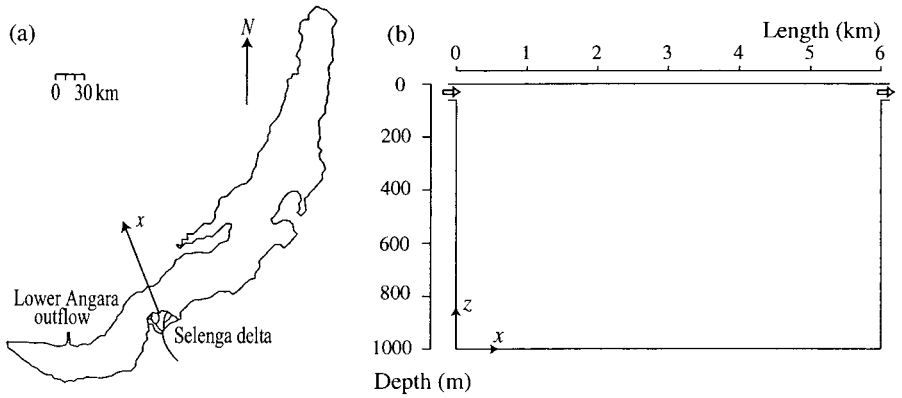

Figure 1. The area to be modelled: (a) Position of section and orientation of x-axis, (b) model domain.

3. Boundary and Initial Conditions

Ascribing appropriate initial and boundary conditions is the principal difficulty in formulating a model of the riverine thermal bar. In particular, including a mass flux through the domain leads to a rather arbitrary choice of outflow condition which then limits the validity of the simulated flows to the period in which the thermal bar is far from the mass sink. Also, salinity and temperature data particular to the Selenga delta are scarce in the western literature. It is emphasised that the conditions presented here are intended to provide an examination of the fundamental dynamics of a generic riverine thermal bar and should therefore be viewed as a first attempt to model the extremely complex buoyancy forcing behind this phenomenon.

The boundary conditions are set as follows. On all solid boundaries

$$u = 0, \quad w = 0, \quad \frac{\partial \Phi}{\partial n} = 0, \tag{8}$$

where n is the direction normal to the boundary in question and $\Phi = T, S, \varphi$.

At the free surface a zero stress condition is used with the rigid-lid approximation, whereby

$$w = 0, \quad \frac{\partial u}{\partial z} = 0, \quad \frac{\partial \Phi}{\partial z} = 0. \tag{9}$$

No surface fluxes of beat, salt or tracer are permitted during the mixing period, so that the dynamics are solely driven by the relative buoyancy characteristics of the river plume and ambient lake.

The river inflow and outflow are simply given a constant horizontal velocity, so

$$u = u_R, \quad \frac{\partial w}{\partial x} = 0 \tag{10}$$

on the open regions shown in Figure 1b. Throughout this study an inflow velocity of $u_R = 5 \times 10^{-3}$ m s^{-1} is used, a value which influences the predicted flows without overpowering buoyancy effects. Together with the 50 m inflow depth, this rather small velocity can be taken as representative of conditions a little distance into the lake, and yields a river discharge rate within the wide range of values documented for the Selenga [4]. The outflow has a Neumann condition on all scalar quantities

$$\frac{\partial \Phi}{\partial x} = 0 \tag{11}$$

but they are explicitly given on the inflow, so that

$$\Phi = \Phi_R \tag{12}$$

there for $\Phi = T, S, \varphi$. It should be noted here that a subscript 'R' denotes a riverine boundary value of the variable in question, while a variable subscripted 'L' refers to a lake value.

The initial and boundary conditions for temperature are generated from the results of one-dimensional models after various simulation times, a procedure which is described in the following section. Salinity is initially assumed to have a homogeneous distribution in the river and lake, at the average Baikal value of $S_L = 96.3$ mg kg^{-1} [27]. The salinity of the Selenga River is given at 126.8 mg kg^{-1} by Votintsev [28] but unfortunately this accurate value is inappropriate for this study because considerable dilution must take place in the shallow delta region between the river mouth and the 50 m-deep inflow of our model. Therefore salinity increases of 1, 2, 5, and 10 mg kg^{-1} are applied to the river while S_L is kept constant. The riverine tracer is allocated river and lake values of $\varphi_R = 1$ and $\varphi_L = 0$ respectively in all simulations.

The flow is supposed to be at rest at the start of the simulation, $u = w = 0$, so Equation (3) becomes the hydrostatic equation:

$$\frac{\partial p}{\partial z} = -\rho g. \tag{13}$$

Since $\rho = \rho(p, S, T)$, Equation (13) has to be solved iteratively under a surface boundary condition of $p = 0$ to obtain initial fields of pressure and density for the given distributions of S and T. The simulation then proceeds with a time increment of $\Delta t = 30$ s from this initial state until the thermal bar has traversed the lake.

4. Thermal Conditions

The studies of cabbeling are intended to show the forcing behind the dynamics of the thermal bar at several stages of the Spring warming process. For this reason the initial conditions for the lake and the boundary conditions for the river need to be as realistic as possible given the Spring warming regime in and around Baikal, so one-dimensional pre-conditioning models are adopted.

These models are based around the unsteady diffusion equation

$$\frac{\partial T}{\partial t} = \frac{\partial}{\partial z}\left(K_v \frac{\partial T}{\partial z}\right), \tag{14}$$

where formulation (7) is adopted for K_v. Radiative heating is simulated through a thermal boundary condition at the surface, which is written in terms of the surface heat flux Q_s as

$$\rho_c c_p K_v \frac{\partial T}{\partial z} = Q_s, \tag{15}$$

where c_p is the specific heat at constant pressure and Q_s is measured in W m^{-2} and is considered positive when entering the domain, directed towards negative z. A value of $Q_s = 250$ W m^{-2} is used throughout the model, which corresponds to the June value given by Shimaraev *et al.* [4]. A percentage of the solar radiation is supposed to pass through the surface to deeper regions of the lake, and the resulting heat source is assumed to have an exponential decay in intensity with depth. The attenuation coefficient associated with this decay is taken to be 0.3 m^{-1}, the value used by Botte and Kay [13].

There is a stage during the Spring warming when the waters of Lake Baikal have an almost uniform temperature of 3.4 °C to a depth of several hundred metres [29]. We therefore adopt an initial temperature of 3.4 °C for both river and lake in our one-dimensional model. Results of this model after 7, 9 and 11 days, when the river is warmer than the T_{md} but the lake is still cooler (see Figure 2), are then used to initialise the two-dimensional studies of the Spring thermal bar. The three scenarios encompass a range of different thermal bar circulations which may be achieved with different thermal forcings. The response of the thermal bar to riverine salinity is then tested by introducing the four values of river salinity to each case.

In order to simplify the discussion, the following nomenclature is adopted to identify each of the 12 different thermal bar simulations in this study. A simulation is referred to as $T\tau S\sigma$, where τ is the number of days of simulation of the one-dimensional river and lake models before mixing and σ is the salinity added to the river in mg kg^{-1}. For example, T9S2 is the case mixed after 9 days with a salinity increase of 2 mg kg^{-1}, corresponding to a riverine salinity of 98.3 mg kg^{-1}.

5. Dynamical Results of the Numerical Experiments

5.1. THE RIVERINE THERMAL BAR

Simulation T9 is chosen to be the reference simulation of the thermal bar due to its position as the intermediate member of the three selected thermal scenarios. After 2 days of simulation a plot of velocity vectors (Figure 3a) shows a clearly-defined thermal bar. The front of a warm, stable river intrusion incorporates the local T_{md}

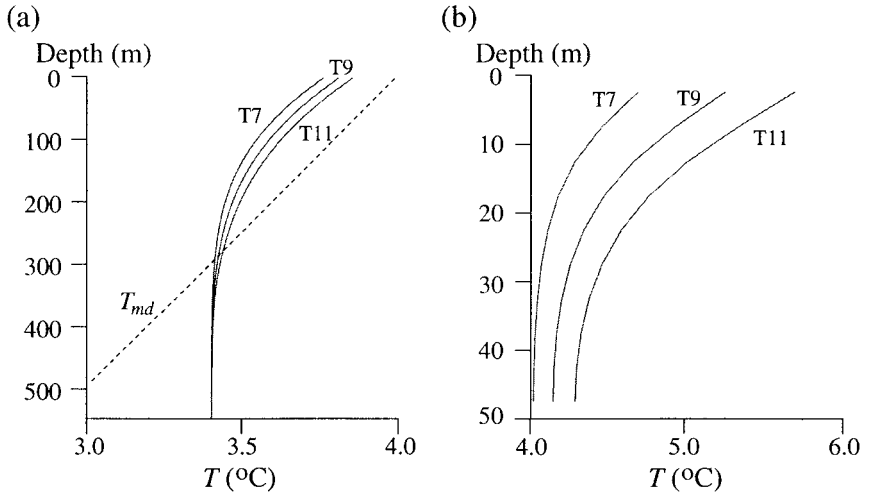

Figure 2. Results of one-dimensional pre-conditioning models for the three thermal scenarios: (a) Initial lake temperatures, (b) river temperatures throughout each mixing simulation.

(which is illustrated as a contour of $T = T_{md}$) and generates a descending plume beneath a surface stagnation point which is surrounded by converging horizontal flows. The stagnation point lags a little behind the surface outcropping of the $T = T_{md}$ contour, probably because of the inertia in the flow ahead of it [30]. The sinking region induces a double-cell circulation which transfers heat and riverine substances downwards into the domain.

In keeping with the numerical results of Malm [1] and the field observations of many other authors [11, 31], all of which are taken from relatively shallow lakes, the isotherms beneath the surface density maximum (ρ_{max}) are deflected back towards the inflow (Figure 3b). In contrast with these works, the size of our domain allows buoyancy forces at depth to drive fluid motion with little interference from bottom boundary effects, and the flow is also deflected backwards in our model. Closer examination of the $T - T_{md}$ contours reveals that the descending plume follows the locus of the densest water at each particular depth, so that the deflection is clearly due to earlier advection of heat downwards by the travelling thermal bar.

The slight deceleration which is observed in the descending flows of Figure 3a exemplifies the effect of thermobaricity on the thermal bar plume. In order to gain an insight into the buoyancy forces responsible for this effect, we define

$$\Delta B = -\frac{g}{\rho_0}(\rho(T, S, p_{in}) - \rho(T_{in}, S_{in}, p_{in})), \tag{16}$$

the change in buoyancy forcing from initial conditions. where subscript '*in*' denotes an initial value.

Figure 4 shows a profile of ΔB at the position of the sinking plume in Figure 3a. Clearly heating causes a large negative buoyancy change (i.e., downwards forcing) above 250 m, but beneath this depth any warming actually increases the buoyancy,

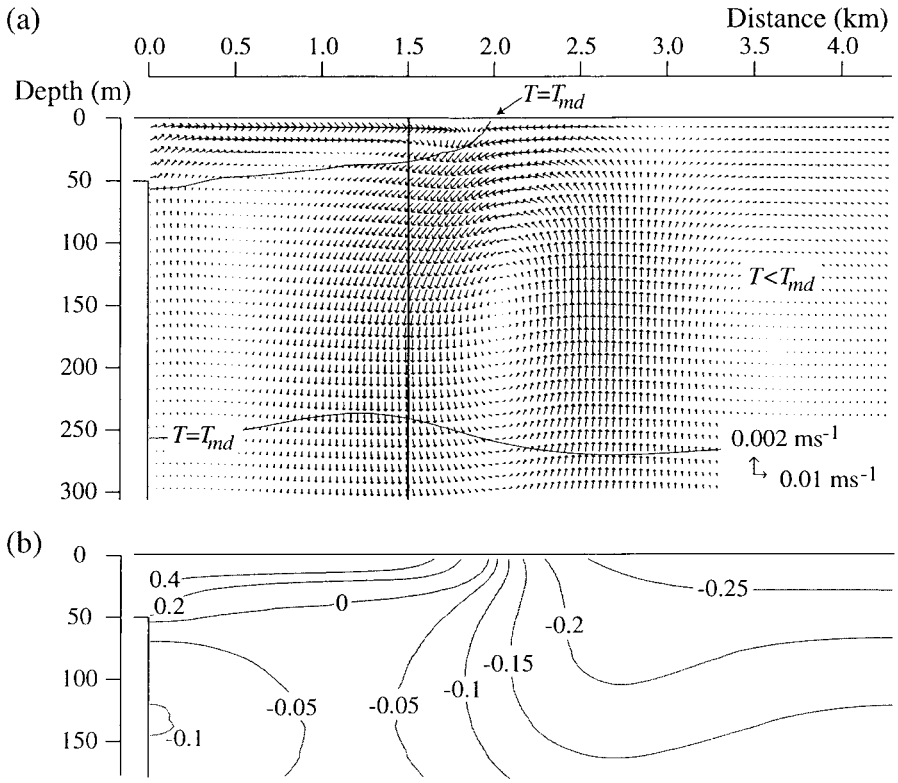

Figure 3. Characteristics of case T9 after 2 days of simulation: (a) Velocity vectors (shown at $\frac{1}{2}$ of the resolution of the model) and $T = T_{md}$ line, (b) contours of $T - T_{md}$. The solid vertical line indicates the position of the profile in Figure 4.

producing an upwards forcing which tends to suppress sinking motions. This arises due to the decrease in the T_{md} with depth; downward transport of water at 4 °C from the surface cabbeling shifts the temperature profile at 300 m depth away from the T_{md} because maximum density is achieved there at about 3.4 °C. This imposes a 'thermobaric barrier' at around 300 m depth; as shown by Carmack and Weiss [9], a non-saline thermal bar cannot penetrate beyond this depth.

As the circulation offshore of the $\rho_{\max}$ grows from the 2-day situation, the horizontal flows converging at the T_{md} reach a balanced state whereby the surface transfer of heat away from the river is halted by return flows and the main advection of heat is in the vertical direction. The thermal bar then remains in a fixed position and warms deeper waters until the whole water column inshore of $\rho_{\max}$ is above the T_{md}. By this stage, thermobaricity ensures that all significant motion is limited to the top 250 m of the domain.

The subsequent flow is shown in Figure 5. The descending plume at about 2 km from the shore encounters the thermobaric barrier and turns to become a horizontal intrusion in the offshore direction at depths of 150–300 m. This necessitates a re-

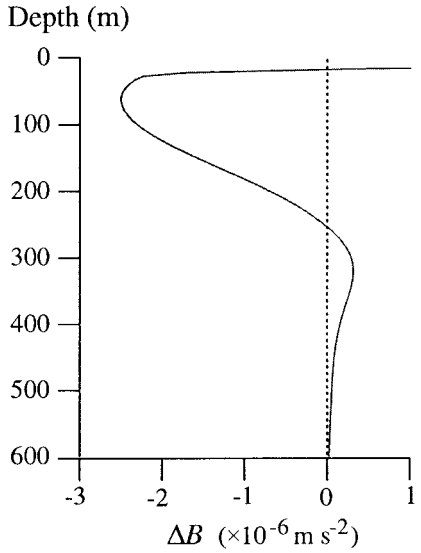

Figure 4. Profile of change in buoyancy force, ΔB, taken 1500 m from left shore in simulation T9.

turn flow of less dense water in the shoreward direction near the surface. A similar combination of a thermal bar with a 'lock-exchange' flow on its offshore side was observed in Marmoush *et al.*'s [32] laboratory experiments.

This analysis regards the T9 thermal bar as a two-stage phenomenon. The first stage features a rapidly-moving thermal bar with a warm river intrusion floating on the cooler lake and downwelling where cabbeling is active. The slower second stage begins when the surface gravity current is balanced by the offshore return flow and the thermal bar can only proceed by gradual warming from the river. This takes place as the river progressively warms the entire epilimnion to above the T_{md} through a horizontal intrusion immediately above the thermobaric barrier.

The thermal bar is quite different in the other simulations. In case T11, the large disparity between $T_{md} - T_L$ and $T_R - T_{md}$ produces a strong surface gravity current with a cabbeling region at its nose. This plume rapidly traverses the lake because the large horizontal density gradient in the stable region inshore of the thermal bar generates motions which totally outweigh the weak return flows on the offshore side of the T_{md} (Figure 6a). The second stage of the T9 circulation therefore never materialises in case T11 and the thermal bar quickly reaches the outflow.

The opposite scenario is found in case T7, where the difference between $T_{md} - T_L$ and $T_R - T_{md}$ is the smallest of the scenarios presented here. The fixed river velocity u_R initially pushes $\rho_{\max}$ away from the inflow, but the circulation offshore of the thermal bar which is generated in response to the cabbeling quickly overcomes the weak density gradient inshore of $\rho_{\max}$ and pushes the thermal bar back to the river mouth to form a boundary plume (Figure 6b). This eventually meets

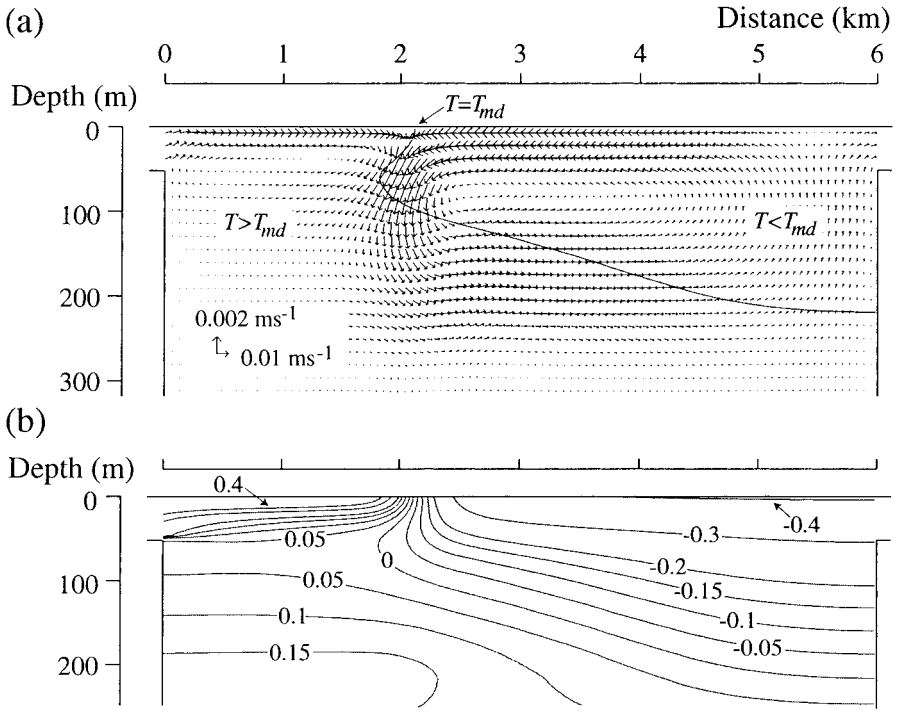

Figure 5. Characteristics of case T9 after 8 days of simulation: (a) Velocity vectors shown at $\frac{1}{3}$ of the resolution of the model, (b) contours of $T - T_{md}$ (°C).

thermobaric resistance and the river water is deflected horizontally away from the boundary under a similar mechanism to the intrusion in the later stages of case T9.

The above observations may be summarised by noting that it is the comparative difference between $\rho_{\max} - \rho_L$ and $\rho_R - \rho_L$ which fixes the flow regime, from cabbeling boundary plume (where the former dominates) to surface gravity current (where the latter is prevalent).

5.2. EFFECTS OF SALINITY

Figure 7a shows the effect of the addition of 1 mg kg^{-1} salinity to the river on the delicately-balanced T9 case. The horizontal propagation of the thermal bar is halted near the inflow as a result of a stronger downwards advection of density-increasing substances, which is explained below. The plume is obviously strengthened by the density increase associated with haline effects because the whole water column is stratified near the inflow after only 2 days.

In order to quantify the relative effects of T and S, it is convenient to introduce two further measures of the change in buoyancy forcing from initial conditions:

$$\Delta B_T = -\frac{g}{\rho_0}(\rho(T, S_{in}, p_{in}) - \rho(T_{in}, S_{in}, p_{in})), \tag{17}$$

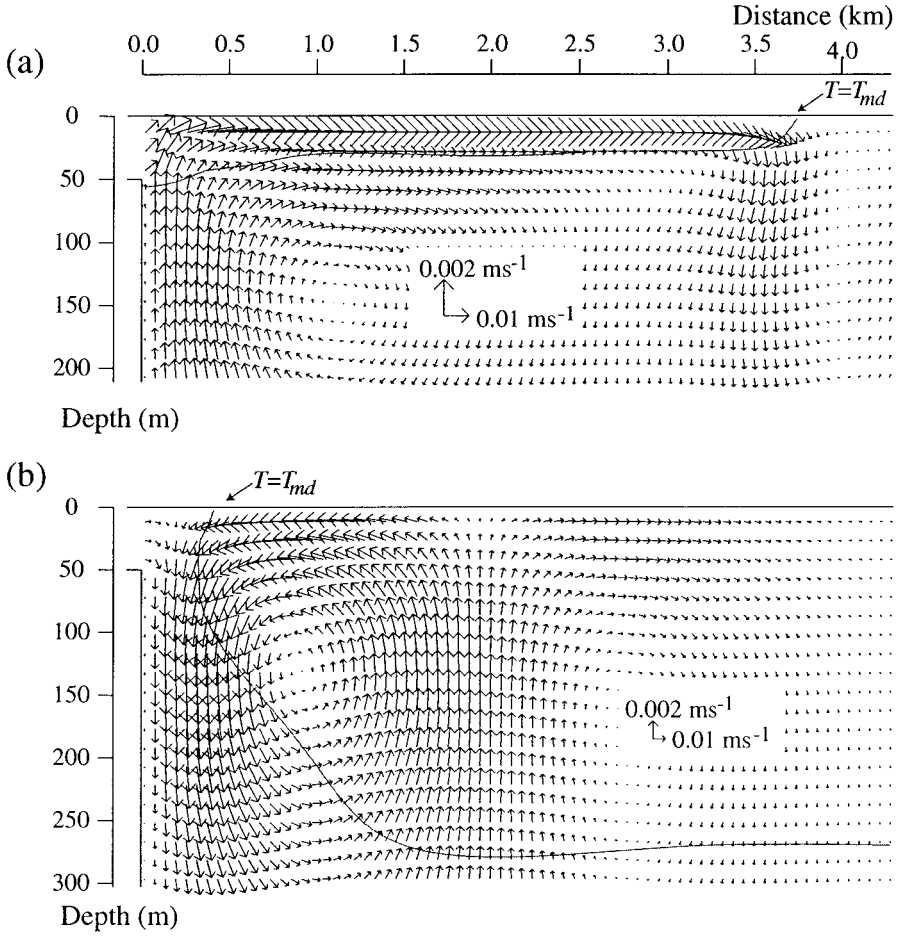

Figure 6. Velocity vectors after 2 days of simulation, shown at $\frac{1}{3}$ of the resolution of the model: (a) Case T11, (b) case T7.

$$\Delta B_S = -\frac{g}{\rho_0}(\rho(T_{in}, S, p_{in}) - \rho(T_{in}, S_{in}, p_{in})), \tag{18}$$

which quantify the buoyancy change due to temperature and salinity respectively.

Plotting all buoyancy measures down the centre of the plume in case T9S1 (Figure 7b) shows the components of buoyancy forcing and illustrates the thermobaric control of sinking within a saline thermal bar. It can be seen that salinity exerts a negative (i.e. downwards) influence on ΔB throughout the plume, while transport of heat to 300 m depth raises the buoyancy there due to thermobaricity. Since ΔB is seemingly influenced more by ΔB_T than ΔB_S, Figure 7b shows that salinity plays an ancillary role to the thermal control of vertical movement in case T9S1.

Increasing the river salinity in cases T9S5 and T9S10 strengthens the downwards flow near the river and increases the maximum depth to which considerable

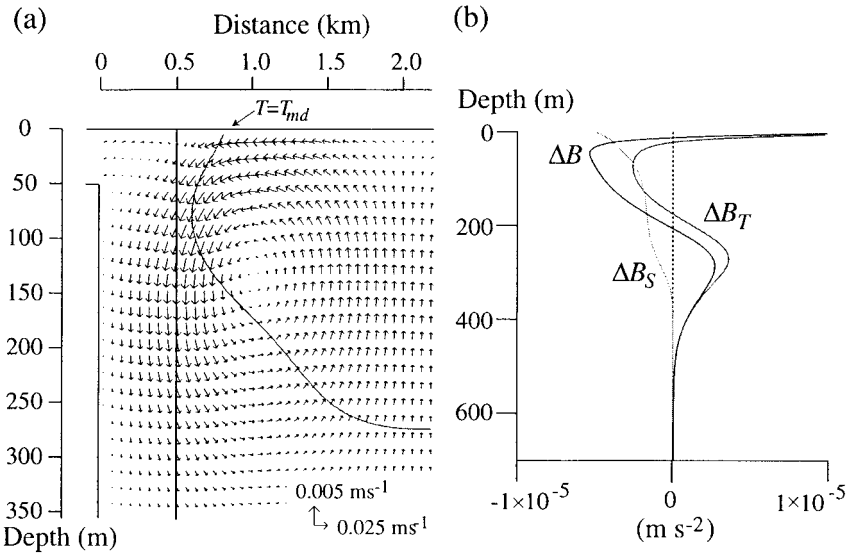

Figure 7. Characteristics of simulation T9S1 after 2 days: (a) Velocity vectors (shown at $\frac{1}{3}$ of the resolution of the model) and $T = T_{md}$ line, (b) buoyancy change measures ΔB, ΔB_T, and ΔB_S, in profile 500 m from left shore. The solid vertical line in (a) indicates the position of the profile in (b).

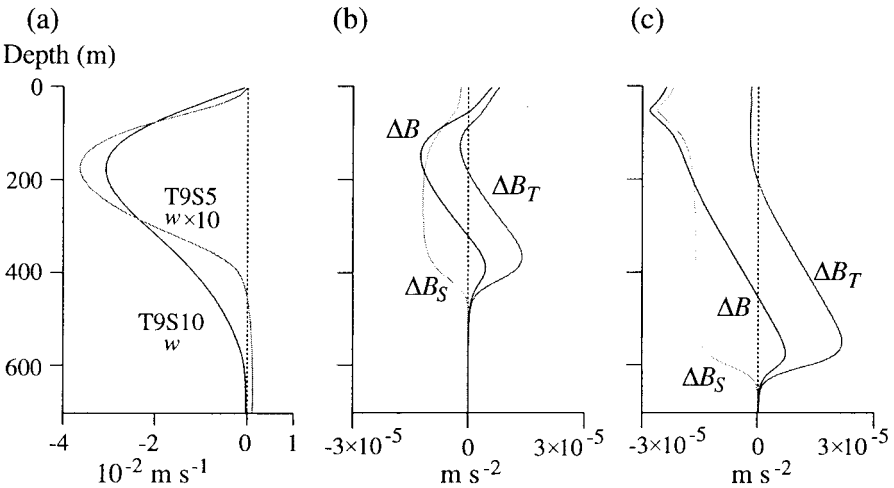

Figure 8. Plume profiles in higher-salinity T9 cases after 2 days, taken at 400 m and 150 m from left shore in cases T9S5 and T9S10 respectively: (a) Vertical velocity, (b) T9S5 buoyancy change, (c) T9S10 buoyancy change.

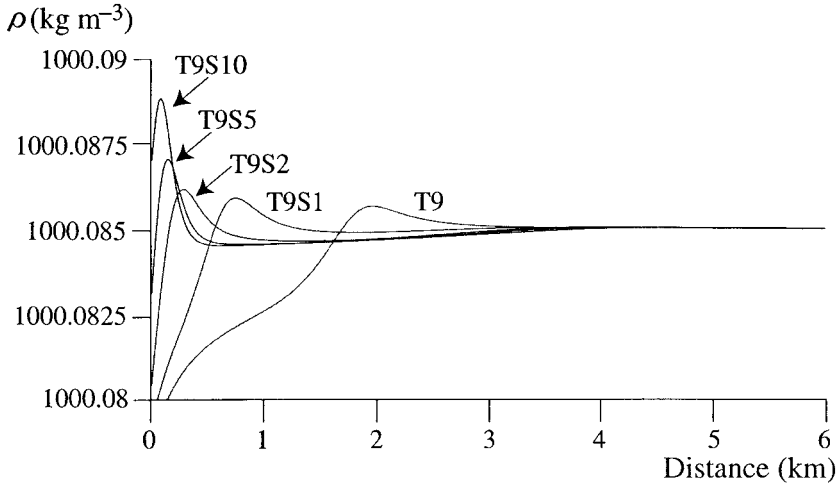

Figure 9. Horizontal density profiles for all saline variants of T9, taken at 10 m depth after 2 days of simulation.

downwelling takes place (Figure 8a). Figures 8b and 8c show why: larger salinities produce more significant changes in buoyancy forcing, which in turn has a more profound effect on vertical flow. The river plume sinks deeper because warm surface waters have to be carried further in order to produce the larger upwards buoyancy forces necessary to counter the increased downwards forcing from salinity.

Figure 9 shows the effects of increasing salinity on the horizontal density distribution of the T9 scenario. Salinity obviously curtails the propagation of the thermal bar by making the plume denser and raising the value of $\rho_{\max}$. Increased sinking near the river mouth delays horizontal propagation because it strengthens the compensating flows directed towards the river inflow at the surface. Widening the density anomaly between plume and lake and decreasing the density difference inshore of the thermal bar also reinforces surface flows and increases downwelling velocities.

The quick propagation of case T11 does not succumb so easily to saline effects, and lower-salinity T11 variants still feature a travelling thermal bar as seen in Figure 10a. However, the main downwelling of this phenomenon takes place only 1 km from the boundary due to an extended version of the deflection mechanism described in Section 5.1 for case T9. Salinity forcing overcomes the surface gravity current in case T11S5 and a boundary plume operates as before (Figure 10b).

Saline experiments on case T7 bear predictable results, since the boundary plume of the non-saline case is simply strengthened with the addition of salinity.

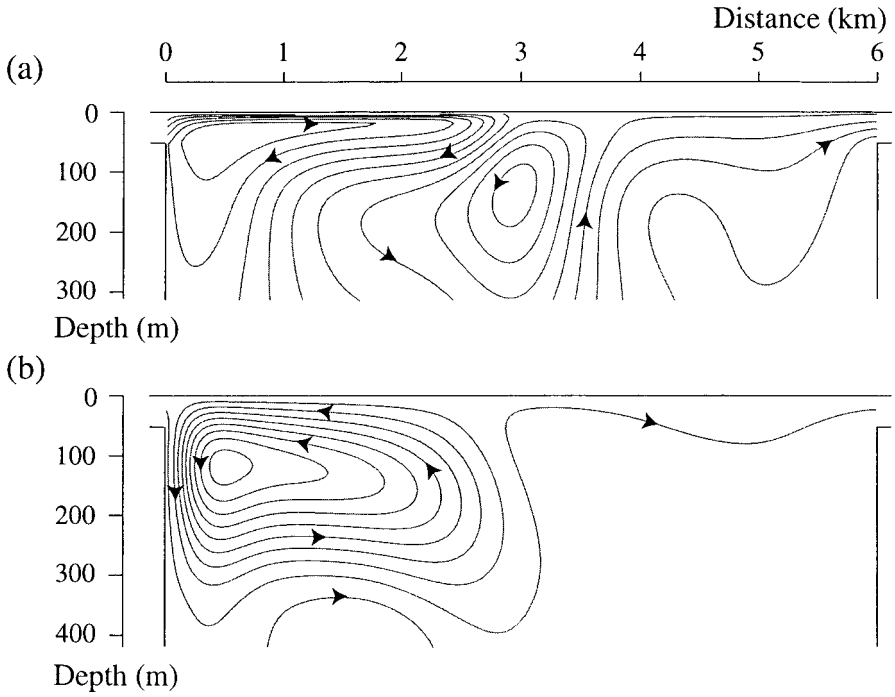

Figure 10. Streamlines of saline T11 variants after 2 days: (a) Case T11S1, (b) case T11S5.

6. Transport of Riverine Substances

The main motivation for this study is to investigate the ability of a thermal bar to transport materials to a greater depth with the addition of salinity than in the purely thermal case. To this end, the riverine tracer φ is introduced to quantify the mixing ratio of river and lake water at every point in the domain.

Isolines of the concentration of the riverine tracer variable φ (Figure 11) provide a useful quantification of the transport of matter by the flows described in the preceding section. Rapid propagation of the thermal bar due to an increased river temperature in T11 clearly leads to the dispersion of riverine materials over a thin surface layer, while the boundary plume generated by case T7 results in vertical transport and little horizontal mixing.

Figure 11 also shows that the addition of a saline buoyancy component significantly curtails horizontal transport at the surface and causes river-borne substances to sink at the boundary. In cases T7S2 and T9S2 this results in a sub-surface plume emanating horizontally away from the boundary as a result of the thermobaric impedance of sinking.

In this section the characteristics of river water mixing by the saline thermal bar are assessed separately in vertical and horizontal directions. These analyses are then related to the questions of deep-water renewal and Spring plankton dynamics, respectively.

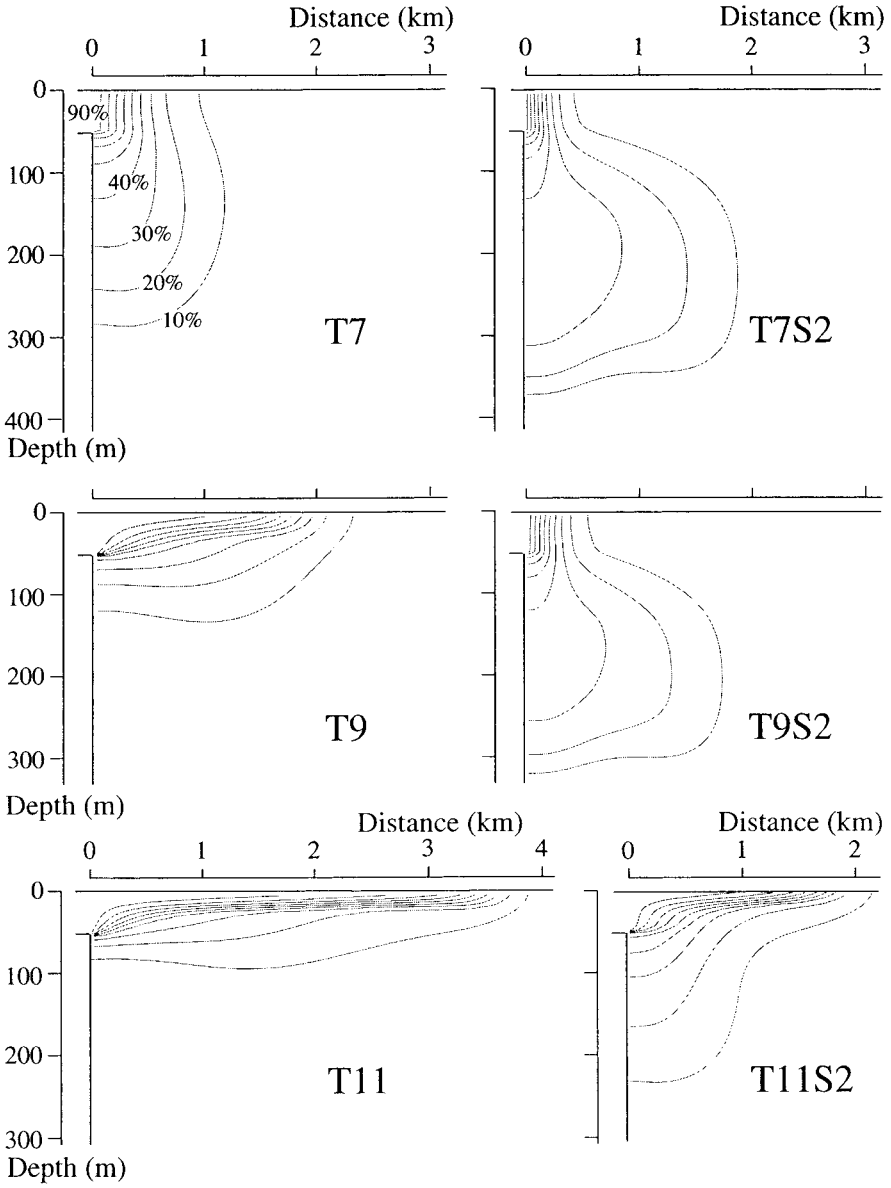

Figure 11. Isolines of riverine tracer concentration in all thermal cases with and without the effects of salinity. Concentration contours are shown at intervals of 10% over the full range of mixed river and lake water.

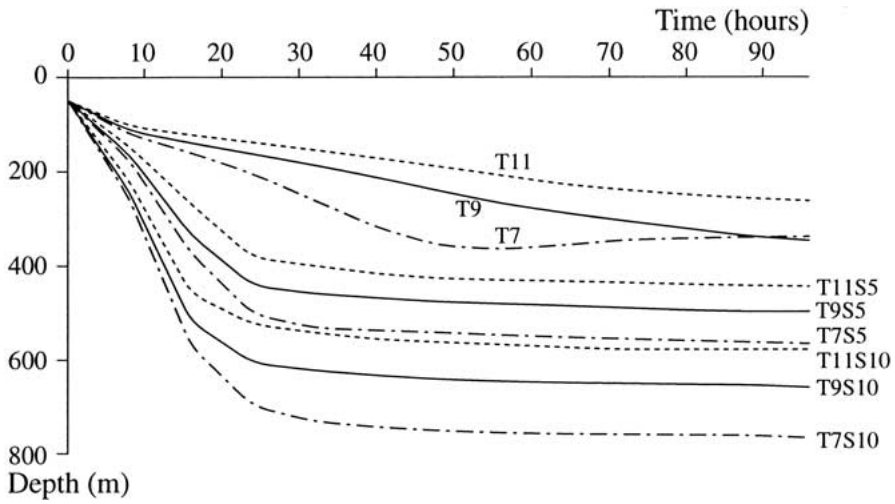

Figure 12. Vertical progression of the 1% concentration of riverine tracer in selected saline cases of all thermal scenarios.

6.1. VERTICAL TRANSPORT

Vertical transport is studied here by recording the maximum depth of a 1% concentration of river water at any horizontal position. This value is chosen to make the tracer representative of specific flows but also relevant to many problems, e.g., riverine pollution, oxygen transport, etc. Numerical testing shows that the maximum depths of other tracer concentration values have a similar tendency. It is emphasised that the study is of vertical transport of water originating in the river, not at the surface as measured in most field studies concerned with deep-water renewal.

Figure 12 charts the progression of vertical tracer penetration in selected saline variants of all thermal cases, showing that riverine substances are mixed into deeper regions far more effectively by a saline thermal bar. The equilibrium achieved by vertical buoyancy forces is represented by the cessation of any further sinking after an initial period of downwards tracer transport, as shown by comparing Figure 12 with Figures 8b and 8c. The progression also reveals that the thermal bars with a higher salinity reach this equilibrium level more quickly, even though it is deeper, because vertical transport is much faster in these cases.

Comparing the three thermal cases over a range of salinities in Figure 12 confirms the expectation that the maximum thermal bar penetration is caused by the highest salinity difference and lowest temperature difference between river and lake. However, the discovery that a simulated saline thermal bar in early Spring (when T_R is still close to the T_{md}) may transport riverine substances to 700 m is by no means trivial. This plot shows that when freshwater temperatures are close to the T_{md}, small variations in salinity can become critically important in determination of the buoyancy forces and capacity for deep-water renewal.

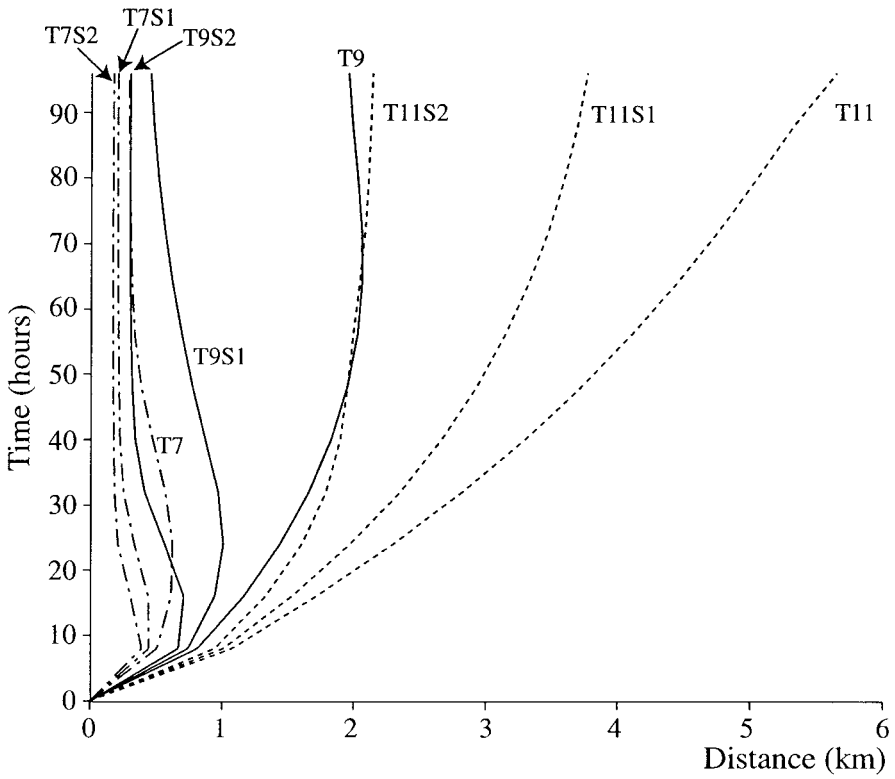

Figure 13. Horizontal progression of the surface waters which are at the T_{md}.

6.2. HORIZONTAL TRANSPORT

The rate of propagation of the riverine thermal bar away from its source is of great importance to the ecology of the river delta region. Suppression of the horizontal spreading of the stable, nutrient-rich waters inshore of the thermal bar would certainly result in reduced phytoplankton productivity [12], potentially heralding a summer of lower growth for every member of the associated food web. Effects of this reduction would probably be localised within the river delta region but may be of great importance to the individual species present in this area.

A concise view of thermal bar progression may be gained by plotting the movement of the surface water at the T_{md} throughout each simulation (Figure 13). The water inshore (to the left) of the resulting progression would then be the stable area favourable for plankton growth.

Figure 13 reveals the drastic reduction in propagation speed which is the result of adding 2 mg kg^{-1} to the river salinity value. In all cases the change in horizontal flows resulting from an addition of salinity confines the inshore stable region to a fraction of its former extent. In some simulations it may be observed that the thermal bar is actually forced to regress towards the river inflow region, as the off-

shore circulation induced by downwelling becomes stronger than flows generated directly adjacent to the river mouth.

All of these observations imply that the addition of salinity to a thermal bar plume will suppress horizontal mixing of riverine substances at the surface and encourage the river plume to transport matter vertically instead. The differences between saline and non-saline thermal bars will therefore produce rather different environments for the flora and fauna of a temperate river delta.

7. Conclusions

A finite-volume formulation of the quasi-incompressible Navier–Stokes equations, adopting a stability-sensitive expression for the vertical eddy-viscosity, is used to investigate the dynamics of the riverine thermal bar in an idealised deep lake under several thermal and haline forcings.

Three thermal scenarios are tested at different stages of the Spring development of a thermal bar, elucidating a range of possible dynamics available to this single phenomenon. The buoyancy forces involved in thermobaric control of a thermal bar's plume are also explicitly illustrated for the first time. In the absence of salinity differences, the depth at which thermobaric control operates is where the initial temperature profile crosses the $T = T_{md}$ profile. If very cold waters were present at all depths, there would be no thermobaric control [33]; however in lake Baikal there is a Winter mid-depth temperature maximum of 3.4–3.6 °C [34], implying thermobaric control at depths of 200–300 m. In general it is important to consider pressure effects in the equation of state of water for lakes deeper than 200 m.

The most significant advance of this work is the evaluation of saline effects on a riverine thermal bar. The curtailment of horizontal propagation of the thermal bar associated with a riverine salinity increase could severely inhibit the dispersion of riverine pollutants and nutrients in a temperate lake, while the increased vertical mixing could substantially increase residence times of these pollutants in the lake [18]. A riverine loading of pollutants which is safe when dispersed throughout the lake could be concentrated to a harmful level when localised by flow patterns within specific regions of a lake. It is therefore important to consider the possible effects of salinity when determining acceptable levels of pollution in a temperate lake.

Of most importance to Baikal is the deepened vertical advection which results from a salinity increase suppressing the thermally-induced resistance to sinking. The thermal bar plume could certainly be involved in deep mixing of Lake Baikal if combined with an increased riverine salinity of the magnitudes studied here.

It has also been shown that the curtailment of horizontal mixing associated with a saline thermal bar could have repercussions on the whole ecosystem of a river delta region. Any reduction in extent of the favourable conditions for plankton growth inshore of the density maximum would obviously have a large effect on the Spring plankton bloom in the vicinity of a thermal bar.

The crucial point is that salinity cannot be ignored in any temperate lake during Spring and Autumn overturn, when temperatures are close to the T_{md}. Neglect of the buoyancy forcings arising from salinity variation in Baikal has been shown here to be flawed, at least when considering regions in the vicinity of a river delta. There is clearly an important range of conditions under which the complex interplay between thermal and haline effects must be included in modelling efforts.

It is hoped that this rather qualitative study will prompt more detailed work into the dynamics of the Selenga region and saline effects on freshwater thermal phenomena in general. Studies are currently underway into the effects of salinity on the thermal bar and plankton populations in a shallower lake throughout the entire Spring warming period, and it is hoped that it will eventually be possible to model the full yearly cycle, incorporating both Spring and Autumn thermal bars.

8. Acknowledgement

This work was funded by the U.K. Natural Environment Research Council under grant number GR3/11029.

References

1. Malm, J.: 1995, Spring circulation associated with the thermal bar in large temperate lakes, *Nordic Hydrol.* **26**, 331–358.
2. Shimaraev, M.N., Granin, N.G. and Zhdanov, A.A.: 1993, Deep ventilation of Lake Baikal due to spring thermal bars, *Limnol. Oceanogr.* **38**, 1068–1072.
3. Zilitinkevich, S.S., Kreiman, K.D. and Terzhevik, A.Y.: 1992, The thermal bar, *J. Fluid Mech.* **236**, 22–47.
4. Shimaraev, M.N., Verbolov, V.I., Granin, N.G. and Sherstyankin, P.P.: 1994, *Physical Limnology of Lake Baikal: A Review*, Print No. 2, Baikal International Center for Ecological Research, Irkutsk–Okayama.
5. Callender, E. and Granina, L.: 1997, Geochemical mass balance of major elements in Lake Baikal, *Limnol. Oceanogr.* **42**, 148–155.
6. Grachev, M.A.: 1994, Formation of the Baikal International Center for ecological research, *Ecol. Int. Bull.* **21**, 75–88.
7. Killworth, P.D., Carmack, E.C., Weiss, R.F. and Matear, R.: 1996, Modelling deep-water renewal in Lake Baikal, *Limnol. Oceanogr.* **41**, 1521–1538.
8. Weiss, R.F., Carmack, E.C. and Koropalov, V.M.: 1991, Deep-water renewal and biological production in Lake Baikal, *Nature* **349**, 665–669.
9. Carmack, E.C. and Weiss, R.F.: 1991, Convection in Lake Baikal: An example of thermobaric instability. In: P.C. Chu and J.C. Garcard (eds.), *Deep Convection and Deep Water Formation in the Oceans*, pp. 215–228, Elsevier Oceanography Series 57.
10. Hohmann, R., Kipfer, R., Peeters, F., Piepke, G., Imboden, D.M. and Shimaraev, N.N.: 1997, Processes of deep-water renewal in Lake Baikal, *Limnol. Oceanogr.* **42**, 841–855.
11. Hubbard, D.W. and Spain, J.D.: 1973, The structure of the early spring thermal bar in Lake Superior. In: *Proceedings of the 16th Conference on Great Lakes Research*, pp. 735–742. Int. Assoc. Great Lakes Res.
12. Moll, R.A., Bratkovitch, A., Chang, W.Y.B. and Pu, P.: 1993, Physical, chemical, and biological conditions associated with the early stages of the Lake Michigan vernal thermal front, *Estuaries* **16**, 92–103.

13. Botte, V. and Kay, A.: 2000, A numerical study of plankton population dynamics in a deep lake during the passage of the Spring thermal bar, *J. Mar. Sys.* **26**, 367–386.
14. Tsvetova, E.A.: 1995, Convective currents associated with the thermal bar of Lake Baikal. In: A.S. Alekseev and N.S. Bakhvalov (eds.), *Advanced Mathematics: Computations and Applications*, pp. 386–393, Novosibirsk Computer Centre, Novosibirsk.
15. Tsvetova, E.A.: 1999, Mathematical modelling of Lake Baikal hydrodynamics, *Hydrobiologia* **407**, 37–43.
16. Carmack, E.C.: 1979, Combined influence of inflow and lake temperatures on spring circulation in a riverine lake, *J. Phys. Oceanogr.* **9**, 422–434.
17. Carmack, E.C., Wiegand, R.C., Daley, R.J., Gray, C.B.J., Jasper, S. and Pharo, C.H.: 1986, Mechanisms influencing the circulation and distribution of water mass in a medium residence time lake, *Limnol. Oceanogr.* **31**, 249–265.
18. Killworth, P.D. and Carmack, E.C.: 1979, A filling-box model of river-dominated lakes. *Limnol. Oceanogr.* **24**, 201–217.
19. Walker, S.J. and Watts, R.G. 1995, A three-dimensional numerical model of deep ventilation in temperate lakes, *J. Geophys. Res.* **100**, 22,711–22,731.
20. Boussinesq, J.: 1903, *Théorie Analytique de la Chaleur*, Vol. 2, Gauthier-Villars, Paris.
21. Chen, C.T.A. and Millero, F.J.: 1986, Precise thermodynamic properties for natural waters covering only the limnological range, *Limnol. Oceanogr.* **31**, 657–662.
22. Imboden, D.M. and Wüest, A.: 1995, Mixing mechanisms in lakes. In: A. Lerman, D. Imboden, and J. Gat (eds.), *Physics and Chemistry of Lakes*, pp. 83–138, Springer-Verlag, Berlin.
23. Welander, P.: 1968, Theoretical forms for the vertical exchange coefficients in a stratified fluid with applications to lakes and seas, *Acta Roy. Soc. Sci. Litt. Gothob. Geophys.* **1**, 1–26.
24. Blackman, R.G. and Tukey, J.W.: 1959, *The Measurement of Power Spectra From the Point of View of Communications Engineering*, Dover Publications, New York.
25. Holland, P.R.: 2001, *Numerical Modelling of the Riverine Thermal Bar*, Ph.D. Thesis, Department of Mathematical Sciences, Loughborough University, U.K.
26. Patankar, S.V.: 1980, Numerical heat transfer and fluid flow. In: *Computational Methods in Mechanics and Thermal Sciences*, Hemisphere, New York.
27. Falkner, K.K., Measures, C.I., Herbelin, S.E., Edmond, J.M. and Weiss, R.F.: 1991, The major and minor element geochemistry of Lake Baikal, *Limnol. Oceanogr.* **36**, 413–423.
28. Votintsev, K.K.: 1993, On the natural conditions of Lake Baikal in connection with the development of its Water Quality Standard', *Water Res.* **20**, 595–604.
29. Botte, V. and Kay, A.: 2001, A model of the wind-driven circulation in Lake Baikal, *Dynam. Atmos. Oceans* (submitted).
30. Farrow, D.E.: 1995, An asymptotic model for the hydrodynamics of the thermal bar, *J. Fluid Mech.* **289**, 129–140.
31. Carmack, E.C., Gray, C.B.J., Pharo, C.H. and Daley, R.J.: 1979, Importance of lake-river interaction on seasonal patterns in the general circulation of Kamloops Lake, British Columbia, *Limnol. Oceanogr.* **24**, 634–644.
32. Marmoush, Y.R., Smith, A.A. and Hamblin, P.F.: 1984, Pilot experiments on thermal bar in lock exchange flow, *J. Energ. Eng.-ASCE* **110**, 215–227.
33. Kay, A.: 2001, Thermobaric flow, *Dynam. Atmos. Oceans* (to appear).
34. Shimaraev, M.N. and Granin, N.G.: 1991, Temperature stratification and the mechanism of convection in Lake Baikal, *Dokl. Akad. Nauk.* **321**, 381–385.